# Propagation Characteristics of Dielectric-Rod-Loaded Waveguides

EDWARD J. ROTHWELL, MEMBER, IEEE, AND LYDELL L. FRASCH, STUDENT MEMBER, IEEE

*Abstract*—**A general technique is presented for calculating the propagation characteristics of a waveguide with arbitrary cross-sectional shape loaded with a circular dielectric rod. The waveguide fields, which are represented as a sum of functions satisfying the homogeneous Helmholtz equation and the boundary conditions at the rod surface, are point-matched at the surface of the waveguide. Numerical examples of a rod centered in a square guide and off center in a circular guide are given, and results for a rod centered in a rectangular cavity are compared with measured data.**

## I. Introduction

THE NEED FOR accurate analyses of waveguides and cavities loaded with dielectric materials is prompted by such diverse applications as the microwave excitation of plasma discharges [1], the measurement of the dielectric properties of materials [2], [3], the modeling of dielectric resonators [4], [5] and millimeter-wave integrated circuit transmission lines [6], [7], and the processing of materials using microwave energy, particularly food [8].

This paper presents a method for calculating the propagation characteristics of a waveguide of arbitrary cross section loaded with a circular dielectric rod. Numerical calculations are based on the point-matching technique, which has been applied successfully to both hollow pipe [9] and dielectric fiber [10], [11] waveguides. Results are given for the dispersion properties of modes in a square guide with a centered dielectric rod, and for the resonant frequencies of a circular cylindrical cavity loaded by an off-center rod. Also, the resonant frequencies of a rectangular cavity with a centered rod are compared with measured values.

## II. Formulation of the Boundary Value Problem

A circular dielectric rod of radius $a$, permittivity $\epsilon_1$, and permeability $\mu_1$ is embedded in a second medium of permittivity $\epsilon_2$ and permeability $\mu_2$, and surrounded by a perfectly conducting sheath, as shown in Fig. 1. Both the rod and the sheath are assumed to be invariant along the waveguiding axis. For simplicity, the waveguide is taken to be symmetric about the $x$ axis, with the axis representing either a magnetic wall (axial electric field even about $x$) or an electric wall (axial electric field odd about $x$). Generalization to the arbitrary asymmetric case is straightforward [11].

Manuscript received May 30, 1987; revised September 8, 1987.

The authors are with the Department of Electrical Engineering and Systems Science, Michigan State University, East Lansing, MI 48824.

IEEE Log Number 8718362.

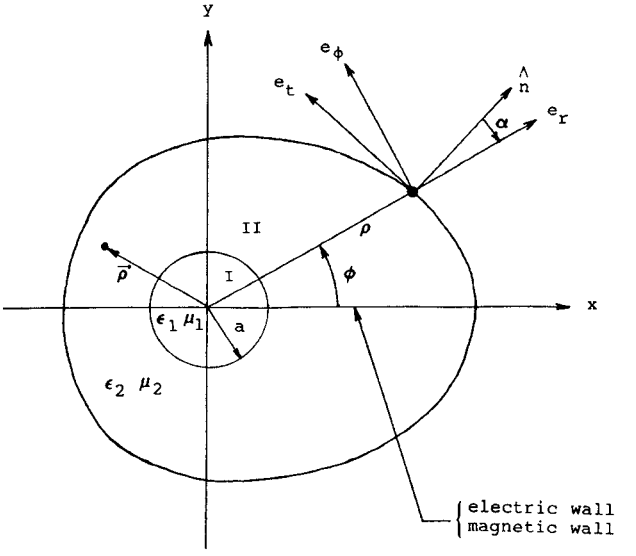


Fig. 1. Geometry of dielectric-rod-loaded waveguide. Cross-sectional shape is general, with symmetry assumed about the $x$ axis.

Since guided wave solutions for the fields in the waveguide are desired, let

$$\vec{E}(\vec{\rho}, z) = \vec{e}(\vec{\rho}) e^{-j\beta z} \qquad \vec{H}(\vec{\rho}, z) = \vec{h}(\vec{\rho}) e^{-j\beta z} \quad (1)$$

where $\vec{\rho}$ is the transverse position vector and $\beta$ is the axial phase constant. The axial modal fields must satisfy the homogeneous Helmholtz equation

$$\left(\nabla_t^2 + k^2\right) \begin{Bmatrix} e_z(\vec{\rho}) \\ h_z(\vec{\rho}) \end{Bmatrix} = 0 \quad (2)$$

in each region of the waveguide, where $\nabla_t$ is the transverse Laplacian and $k^2 = \omega^2 \mu \epsilon$. A separation of variables solution to (2) in cylindrical coordinates results in

$$\begin{Bmatrix} e_z(\vec{\rho}) \\ h_z(\vec{\rho}) \end{Bmatrix} = \left[C_1 B_{k_\phi}^{(1)}(k_r r) + C_2 B_{k_\phi}^{(2)}(k_r r)\right] \times \left[C_3 \cos(k_\phi \phi) + C_4 \sin(k_\phi \phi)\right] \quad (3)$$

where $B_{k_\phi}^{(1)}$ and $B_{k_\phi}^{(2)}$ are appropriate first- and second-kind solutions to Bessel's equation, and $k_r^2 = k^2 - \beta^2$. The periodic nature of the fields in each region requires that $k_\phi$ be an integer. Thus, satisfactory solutions for the axial fields

in each region are given by

$$e_{z1}(\vec{\rho}) = \sum_{n=0}^{\infty} a_n \psi_n(\chi r) F_n(\phi)$$

$$h_{z1}(\vec{\rho}) = \sum_{n=0}^{\infty} b_n \psi_n(\chi r) G_n(\phi)$$

$$e_{z2}(\vec{\rho}) = \sum_{n=0}^{\infty} [c_n \Phi_n(\tau r) + d_n \Theta_n(\tau r)] F_n(\phi)$$

$$h_{z2}(\vec{\rho}) = \sum_{n=0}^{\infty} [e_n \Phi_n(\tau r) + f_n \Theta_n(\tau r)] G_n(\phi) \quad (4)$$

where

$$\chi = \left(|k_{r1}^2|\right)^{1/2} \qquad \tau = \left(|k_{r2}^2|\right)^{1/2} \quad (5)$$

$$\psi_n(\chi r) = \begin{cases} J_n(\chi r) & k_{r1}^2 \geq 0 \\ I_n(\chi r) & k_{r1}^2 < 0 \end{cases} \quad (6)$$

$$\Phi_n(\tau r) = \begin{cases} J_n(\tau r) & k_{r2}^2 \geq 0 \\ I_n(\tau r) & k_{r2}^2 < 0 \end{cases} \quad (7)$$

$$\Theta_n(\tau r) = \begin{cases} Y_n(\tau r) & k_{r2}^2 \geq 0 \\ K_n(\tau r) & k_{r2}^2 < 0 \end{cases} \quad (8)$$

$$F_n(\phi) = \begin{cases} \cos(n\phi) & \text{even modes} \\ \sin(n\phi) & \text{odd modes} \end{cases} \quad (9)$$

$$G_n(\phi) = \begin{cases} \sin(n\phi) & \text{even modes} \\ \cos(n\phi) & \text{odd modes.} \end{cases} \quad (10)$$

Here $J_n$ and $Y_n$ are Bessel functions of the first and the second kind, respectively, and $I_n$ and $K_n$ are modified Bessel functions of the first and the second kind. Note that for even modes the terms in (4) involving $G_0$ are excluded, while for odd modes the terms involving $F_0$ are excluded.

The transverse fields in each region can be calculated [12] via

$$e_r = \frac{-j\beta}{k^2-\beta^2}\left[\frac{\partial e_z}{\partial r} + \left(\frac{\omega\mu}{\beta r}\right)\frac{\partial h_z}{\partial \phi}\right]$$

$$e_\phi = \frac{-j\beta}{k^2-\beta^2}\left[\frac{1}{r}\frac{\partial e_z}{\partial \phi} - \left(\frac{\omega\mu}{\beta}\right)\frac{\partial h_z}{\partial r}\right]$$

$$h_r = \frac{-j\beta}{k^2-\beta^2}\left[-\left(\frac{k^2}{\omega\mu\beta r}\right)\frac{\partial e_z}{\partial \phi} + \frac{\partial h_z}{\partial r}\right]$$

$$h_\phi = \frac{-j\beta}{k^2-\beta^2}\left[\left(\frac{k^2}{\omega\mu\beta}\right)\frac{\partial e_z}{\partial r} + \frac{1}{r}\frac{\partial h_z}{\partial \phi}\right]. \quad (11)$$

The boundary conditions on the tangential components of the electric and magnetic fields require the continuity of $e_z$, $e_\phi$, $h_z$, and $h_\phi$ at $r = a$. Substituting (4) into (11), enforcing these boundary conditions, and employing the orthogonality of the sinusoids allows the amplitude coefficients $a_n$, $b_n$, $c_n$, and $e_n$ to be written in terms of $d_n$ and $f_n$. The axial and transverse components of the electric field in region II can then be written in terms of normalized quantities as

$$e_{z2} = \sum_{n=0}^{\infty} \{\bar{d}_n \Gamma_n(\tau r) + \bar{f}_n Q_{2n} \Phi_n(\tau r)\} F_n(\phi) \quad (12)$$

$$e_{r2} = \sum_{n=0}^{\infty} \frac{-j}{(k_{r2}a)^2}\left\{\bar{d}_n\left[(\beta a)(\tau a)\Gamma_n'(\tau r) + \frac{\sigma_n}{r/a}(k_2 a)\eta_2 Q_{3n}\Phi_n(\tau r)\right] + \bar{f}_n\left[(\beta a)(\tau a)\Phi_n'(\tau r) + \frac{\sigma_n}{r/a}(k_2 a)\eta_2 \zeta_n(\tau r)\right]\right\} F_n(\phi) \quad (13)$$

$$e_{\phi 2} = \sum_{n=0}^{\infty} \frac{j}{(k_{r2}a)^2}\left\{\bar{d}_n\left[\frac{\sigma_n}{r/a}(\beta a)\Gamma_n(\tau r) + (k_2 a)(\tau a)\eta_2 Q_{3n}\Phi_n'(\tau r)\right] + \bar{f}_n\left[\frac{\sigma_n}{r/a}(\beta a) Q_{2n}\Phi_n(\tau r) + (k_2 a)(\tau a)\eta_2 \zeta_n'(\tau r)\right]\right\} G_n(\phi) \quad (14)$$

where

$$\bar{d}_n = \frac{d_n}{R_n} \qquad \bar{f}_n = \frac{f_n}{R_n} \quad (15)$$

$$\sigma_n = \begin{cases} +n & \text{even modes} \\ -n & \text{odd modes} \end{cases} \quad (16)$$

$$\eta = \sqrt{\frac{\mu}{\epsilon}} \quad (17)$$

and the quantities $\Gamma_n$, $\zeta_n$, and $R_n$ and the $Q_n$ terms are given in the Appendix. Here a prime (′) indicates differentiation of Bessel functions with respect to their arguments.

Application of the remaining boundary conditions at the conducting sheath determines the propagation characteristics of the guide. Here the requirement is that the tangential electric fields be zero, or

$$e_{z2} = 0$$

$$e_{t2} = e_{r2}\sin(\alpha) + e_{\phi 2}\cos(\alpha) = 0 \quad (18)$$

for all points on the sheath. The quantity $\alpha$ describes the angle between the radial line and the normal vector at a point on the sheath, as shown in Fig. 1. Note that the eigenvalue equation for the modes of a circular waveguide of radius $b$ with a centered dielectric rod is easily recovered by forcing $e_{z2} = e_{\phi 2} = 0$ at $r = b$.

Application of the boundary conditions (18) can be made tractable by truncating the infinite series in (4) to $N$ terms and matching (18) at $N$ discrete points on the sheath boundary. The result is a homogeneous system of $2N$ linear equations in the $2N$ unknown amplitude coefficients

$\bar{d}_n$ and $\bar{f}_n$, a solution to which is guaranteed only if the determinant of the matrix of coefficients is zero. With $\omega$ fixed, this occurs only at certain values of $\beta$, which are subsequently taken to be the phase constants of the guide.

## III. Conditions at Cutoff

The behavior of the rod-loaded guide at cutoff ($\beta = 0$) is particularly interesting in that it helps classify the mode types away from cutoff. With $\beta = 0$, the boundary conditions (18) reduce to

$$\sum_{n=0}^{\infty} \tilde{d}_n \left[ P_{5n} Y_n(\tau r) - P_{6n} J_n(\tau r) \right] F_n(\phi) = 0 \qquad (19)$$

$$\sum_{n=0}^{\infty} \tilde{f}_n \Bigg\{ \frac{\sigma_n}{r/a} \left[ P_{3n} Y_n(\tau r) - P_{4n} J_n(\tau r) \right] F_n(\phi) \sin(\alpha) - (\tau a) \left[ P_{3n} Y_n'(\tau r) - P_{4n} J_n'(\tau r) \right] G_n(\phi) \cos(\alpha) \Bigg\} = 0 \qquad (20)$$

where

$$\tilde{d}_n = P_{3n} \bar{d}_n \qquad \tilde{f}_n = P_{5n} \bar{f}_n \qquad (21)$$

with the $P_n$ functions given in the Appendix.

It is seen that the expansion coefficients $\tilde{d}_n$ and $\tilde{f}_n$ are no longer coupled by the boundary conditions, and thus it is expected that modes exist which satisfy either (19) or (20) independently. Reference to the original field expansions (4) reveals that the boundary condition (19) can be obtained with $h_{z1} = h_{z2} = 0$ while (20) can be obtained with $e_{z1} = e_{z2} = 0$. Thus, solutions for the cutoff frequency arising from (19) represent modes purely TM to $z$ at cutoff, while solutions obtained using (20) represent modes purely TE to $z$ at cutoff. From this, the nomenclature used to describe hybrid modes away from cutoff is taken to be "HE" if the mode is TE at cutoff and "EH" if the mode is TM at cutoff. It is found that these modes revert to the TE and TM modes of the homogeneously loaded waveguide when $\epsilon_1 \to \epsilon_2$, or $a \to 0$. Also anticipated are modes which are hybrid TE/TM even at cutoff. These modes require (19) and (20) to hold simultaneously and do not correspond directly to modes of the homogeneously filled guide.

## IV. Numerical Examples

As a first example, a square waveguide with a centered dielectric rod is considered. The guide geometry is shown in Fig. 2(a). Fig. 3 shows the cutoff frequencies plotted versus rod radius. The subscript on the mode designation corresponds to the empty waveguide TE or TM mode to which the modes revert at zero rod radius, the first six of which are shown. Since the guide exhibits fourfold symmetry, the first superscript indicates whether the axial field is either even or odd about the $x$ axis, while the second superscript indicates whether even or odd harmonics are used in the axial electric field expansion in (4). With the symmetry states properly identified, point matching on the boundary is required only in the first quadrant. Those modes with eightfold symmetry (e.g. $HE_{11}^{ee}$) require matching only in the first octant.

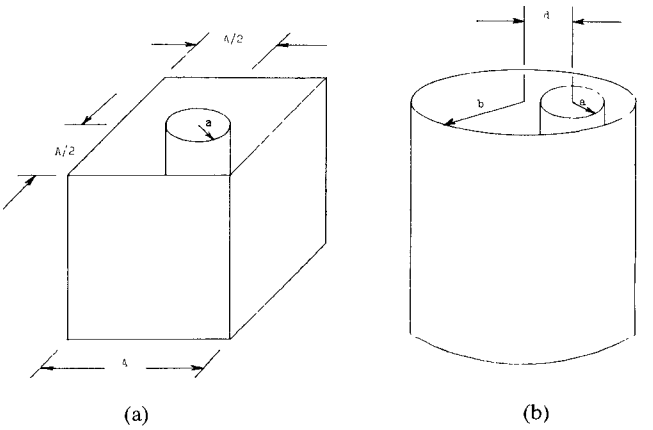


Fig. 2. Geometry of (a) square waveguide with rod on axis and (b) circular waveguide with rod off axis.

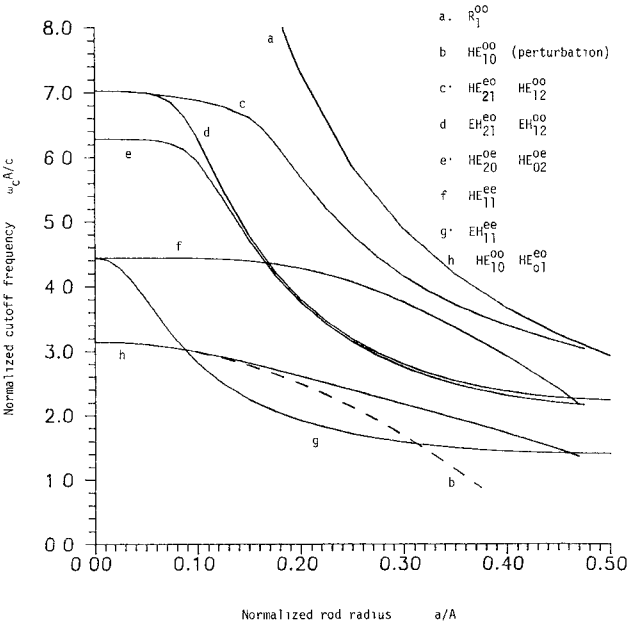


Fig. 3. Cutoff frequencies of square guide with centered dielectric rod versus rod radius for $\epsilon_{r1} = 10$, $\epsilon_{r2} = 1$.

It is seen that as the rod radius is increased, the cutoff frequencies decrease at various rates, with the degenerate modes of the empty guide splitting into modes with distinct separate cutoff frequencies. For $a/A > 0.09$, the $EH_{11}^{ee}$ mode becomes the dominant mode of the guide. A first-order perturbation solution for the cutoff frequency of the $HE_{10}^{oo}$ mode [13] is indicated by the dotted line. This solution is seen to become quite inaccurate when $a/A > 0.2$. Figs. 4 and 5 show the axial field distributions in the guide at cutoff for the $EH_{11}^{ee}$ and $HE_{10}^{oo}$ modes, respectively, constructed from (4). As the permittivity of the rod is increased, the fields are perturbed away from the sinusoidal distributions of the empty guide.

Also displayed in Fig. 3 is a mode with the designation $R_1^{oo}$. This mode is the first encountered which is hybrid TE–TM at cutoff, and does not revert to an empty waveguide mode as the rod radius is reduced to zero. It is termed a rod mode since the cutoff characteristics of the

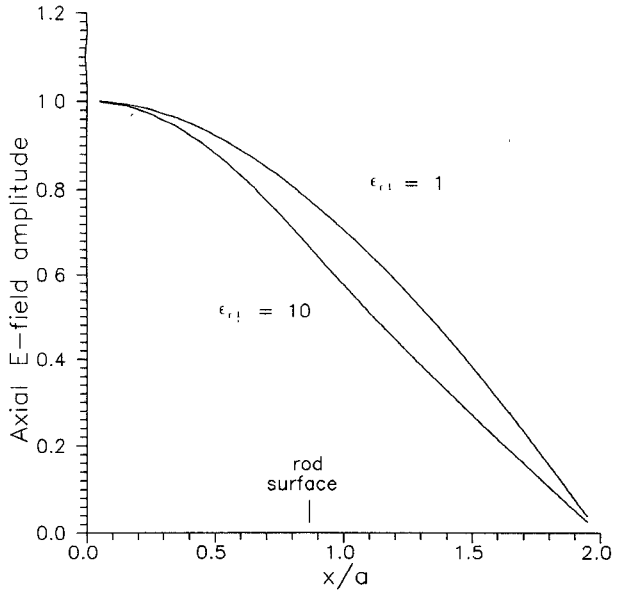


Fig. 4. Axial electric field distributions for $EH_{11}^{ee}$ mode at cutoff in square waveguide with centered dielectric rod, for $y/a = 0.5$, $\epsilon_{r2} = 1$, $A/a = 4$.

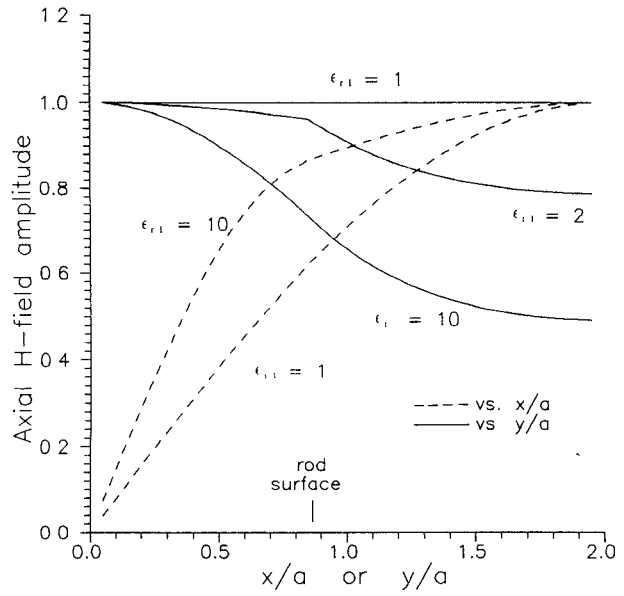


Fig. 5. Axial magnetic field distributions for $HE_{10}^{oo}$ mode at cutoff in square waveguide with centered dielectric rod versus $y/a$ with $x/a = 0.5$ and versus $x/a$ with $y/a = 0.5$, for $\epsilon_{r2} = 1$, $A/a = 4$.

guide are dependent only on the properties of the rod. That is, the cutoff wavenumber of the guide normalized to the rod radius is found to remain constant at $k_c a = 1.46$ regardless of $A/a$, the size of the guide relative to the radius of the rod.

The rod mode is also interesting in that it displays backward-wave behavior. This is readily seen in Fig. 6, which shows the dispersion characteristics of the rod-loaded square waveguide. Whereas most of the modes demonstrate the positive dispersion typical of axially invariant waveguides, the rod mode has a region where the slope of the dispersion curve is negative, indicating that the direc-

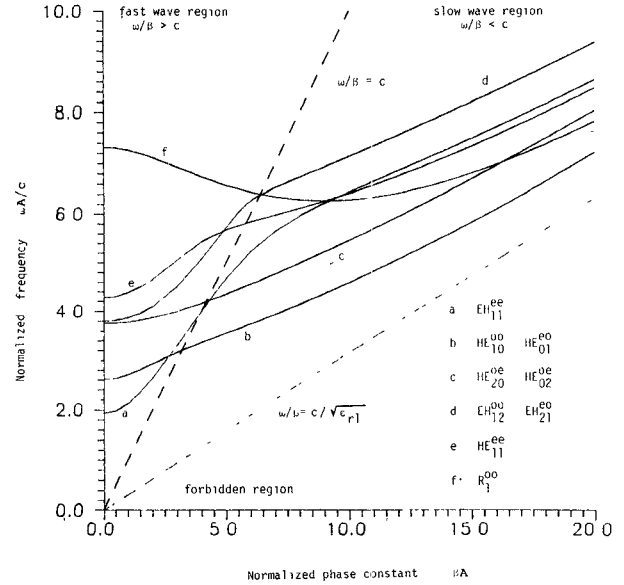


Fig. 6. Dispersion characteristics of square waveguide with centered dielectric rod for $\epsilon_{r1} = 10$, $\epsilon_{r2} = 1$, $A/a = 5$.

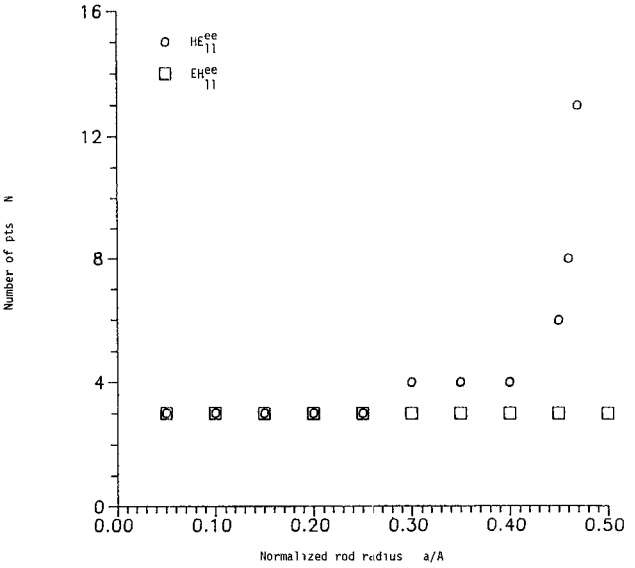


Fig. 7. Number of points in first octant of square waveguide with centered dielectric rod required to calculate cutoff frequency to 1 percent accuracy, versus rod radius, for $\epsilon_{r1} = 10$, $\epsilon_{r2} = 1$.

tion of energy propagation is opposite the direction of phase front propagation. This type of behavior has been previously identified in circular waveguides with axial dielectric rods [14] and in rectangular waveguides with rectangular dielectric rods [15], and has been treated generally in [16]. Interestingly, the dispersion characteristics of the rod mode are also independent of $A/a$. That is, for a given $k_0 a$, $\beta a$ does not depend on the size of the guide relative to the rod radius.

Each of the curves in Figs. 3 and 6 was generated on an IBM PC microcomputer by solving either (18) or (19) and (20) using 20 equally spaced matched points and 20 harmonics. A measure of the sensitivity of the results to the number of matching points is shown in Fig. 7. It is

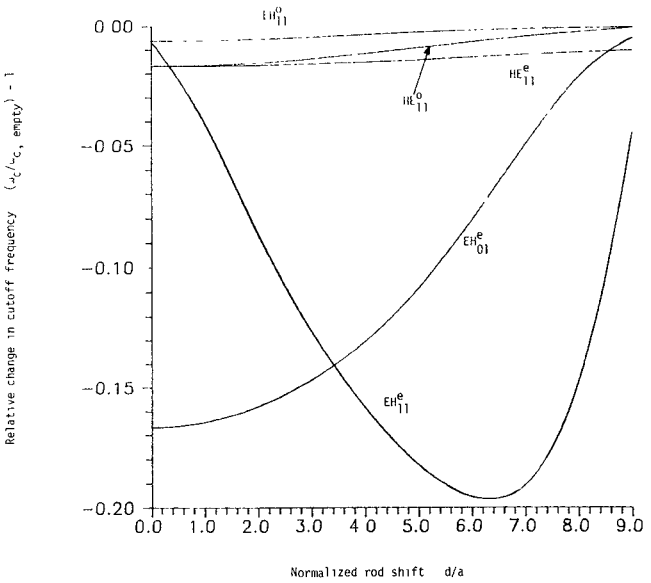


Fig. 8. Change in cutoff frequency from empty waveguide value for dielectric rod placed off center in circular waveguide versus off-center position, for $\epsilon_{r1}=10$, $\epsilon_{r2}=1$, $b/a=10$.

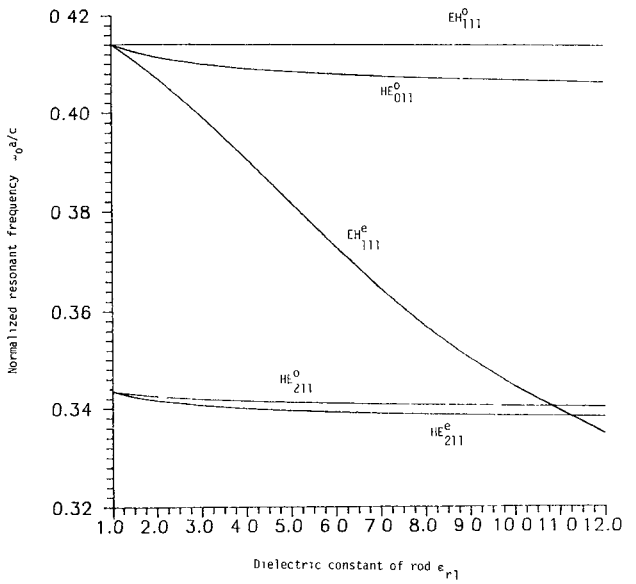


Fig. 9. Resonant frequency of circular cavity loaded off center by dielectric rod, for length $L=2b$, $\beta b=\pi/2$, versus rod dielectric constant, for $\epsilon_{r2}=1$, $b/a=10$, $d/a=6$.

seen that as the rod radius is increased, it takes more matching points (and expansion functions) to calculate the cutoff frequency of the $HE_{11}^{ee}$ mode to within a desired accuracy, while the $EH_{11}^{ee}$ mode is relatively insensitive to the number of points chosen.

As a second example, Fig. 8 shows the change in cutoff frequency which results when a dielectric rod is placed off axis in a circular guide, as shown in Fig. 2(b). Again, the subscript on the mode designation corresponds to the empty waveguide TE or TM mode to which the modes revert at zero rod radius. The superscript is used to indicate whether the axial fields are even or odd about the $x$ axis. Because of the twofold symmetry, point matching is required only in the upper half of the guide. Calculations were done using 20 equally spaced points.

For a rod placed in the center of the circular guide, each of the modal cutoff frequencies is lowered. As the rod is shifted off axis, most of the modes split into two separate cases, demonstrating either even or odd symmetry. Those modes which are azimuthally symmetric when the rod is centered do not split. This is sensible, since the field patterns of these modes are independent of the radial direction along which the rod is to be moved.

It is interesting to see from Fig. 8 that the cutoff frequency of the $EH_{11}^{e}$ mode is highly perturbed as the rod is moved off axis, while the $EH_{11}^{o}$ mode is quite insensitive to shifts in the rod position. This suggests that a cylindrical cavity oscillating in the $EH_{11}^{e}$ mode might be useful for monitoring the dielectric constant of a rod placed off axis. Fig. 9 shows the resonant frequency of a circular cylindrical cavity with an off-axis dielectric rod plotted against the dielectric constant of the rod. It is seen that for $1 \leqslant \epsilon_{r1} \leqslant 10$, the resonant frequency of the $EH_{111}^{e}$ mode varies in a near linear fashion with $\epsilon_{r1}$. The modes nearest in resonant frequency to the $EH_{111}^{e}$ mode, including the $EH_{111}^{o}$ mode, are nearly invariant with changes in $\epsilon_{r1}$, and provide benchmark frequencies.

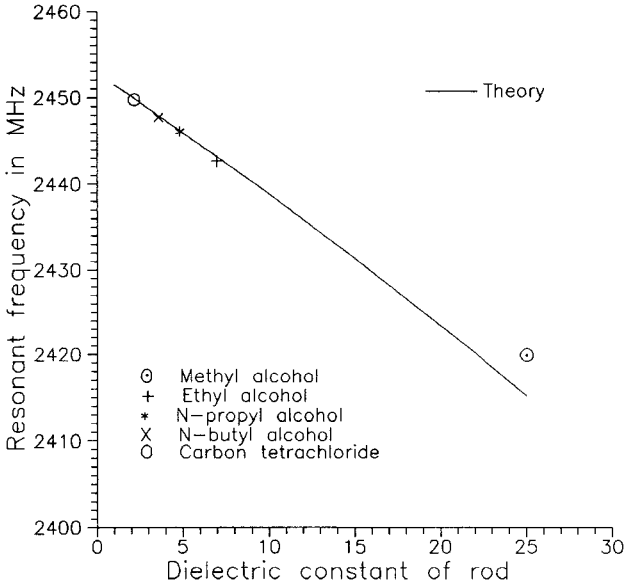


Fig. 10. Comparison of calculated and measured resonant frequencies of 1.7 in×3.4 in×10.2 in rectangular cavity oscillating in $TM_{310}$ mode with centered dielectric sample. Experimental values are from [17].

## V. Comparison to Experiment

To judge the validity of the technique presented in this paper, results are compared with measurements made by Rzepecka [17] of the resonant frequency of a rectangular cavity loaded by a cylindrical sheath containing liquids of various permittivities. His cavity is constructed from a 10.2 in section of WR340 waveguide (3.4 in×1.7 in inner dimensions) and is operated in the 103 mode TE to the axis of the waveguide. The cylindrical dielectric sample is

inserted through a hole in the center of the broad wall, and extends across the waveguide, perpendicular to its axis.

For the purpose of analysis, the cavity can also be viewed as oscillating in the 310 mode TM to the axis of the rod, corresponding to a section of 10.2 in×3.4 in waveguide operating in the $TM_{31}$ mode at cutoff. The resonant frequency does not depend on the length of the guide because the transverse electric fields are identically zero at cutoff (see (13) and (14)).

Fig. 10 shows the $TM_{310}$ resonant frequency of the cavity loaded with a dielectric rod of diameter 0.11 in plotted versus rod permittivity, calculated by solving (19) with ten matching points along the $x$ axis and three points along the $y$ axis. Also shown are Rzepecka's measurements. With the theoretical curve scaled to account for the presence of the insertion hole and the sample holder, agreement is seen to be excellent.

## VI. Conclusions

A technique for calculating the propagation characteristics of dielectric-rod-loaded waveguides has been presented. The technique is numerically simple and computationally rapid. A typical point on a dispersion curve calculated using 20 matching points takes 5 seconds on an IBM PC with a math coprocessor. Numerical results have been presented which demonstrate the usefulness of the technique, and the validity of the technique has been verified by comparison to measured data.

## Appendix

$$\Gamma_n(\tau r) = Q_{1n}\Phi_n(\tau r) + R_n\Theta_n(\tau r)$$
$$\zeta_n(\tau r) = Q_{4n}\Phi_n(\tau r) + R_n\Theta_n(\tau r) \tag{A1}$$

$$Q_{1n} = P_{2n}P_{7n} - P_{3n}P_{6n}$$
$$Q_{2n} = P_{4n}P_{7n} - P_{3n}P_{8n}$$
$$Q_{3n} = P_{6n}P_{1n} - P_{5n}P_{2n}$$
$$Q_{4n} = P_{8n}P_{1n} - P_{5n}P_{4n}$$
$$R_n = P_{3n}P_{5n} - P_{1n}P_{7n} \tag{A2}$$

$$P_{1n} = \left[\frac{1}{(k_{r1}a)^2} - \frac{1}{(k_{r2}a)^2}\right](\beta a)\sigma_n\Phi_n(\tau a)\psi_n(\chi a)$$

$$P_{2n} = \left[\frac{1}{(k_{r1}a)^2} - \frac{1}{(k_{r2}a)^2}\right](\beta a)\sigma_n\Theta_n(\tau a)\psi_n(\chi a)$$

$$P_{3n} = \left[\eta_1\frac{(k_1a)(\chi a)}{(k_{r1}a)^2}\psi_n'(\chi a)\Phi_n(\tau a) - \eta_2\frac{(k_2a)(\tau a)}{(k_{r2}a)^2}\psi_n(\chi a)\Phi_n'(\tau a)\right]$$

$$P_{4n} = \left[\eta_1\frac{(k_1a)(\chi a)}{(k_{r1}a)^2}\psi_n'(\chi a)\Theta_n(\tau a) - \eta_2\frac{(k_2a)(\tau a)}{(k_{r2}a)^2}\psi_n(\chi a)\Theta_n'(\tau a)\right]$$

$$P_{5n} = \left[-\frac{1}{\eta_1}\frac{(k_1a)(\chi a)}{(k_{r1}a)^2}\psi_n'(\chi a)\Phi_n(\tau a) + \frac{1}{\eta_2}\frac{(k_2a)(\tau a)}{(k_{r2}a)^2}\psi_n(\chi a)\Phi_n'(\tau a)\right]$$

$$P_{6n} = \left[-\frac{1}{\eta_1}\frac{(k_1a)(\chi a)}{(k_{r1}a)^2}\psi_n'(\chi a)\Theta_n(\tau a) + \frac{1}{\eta_2}\frac{(k_2a)(\tau a)}{(k_{r2}a)^2}\psi_n(\chi a)\Theta_n'(\tau a)\right]$$

$$P_{7n} = -P_{1n} \qquad P_{8n} = -P_{2n}. \tag{A3}$$

## References


[1] R. Mallavarpu, J. Asmussen, and M. C. Hawley, "Behavior of a microwave cavity discharge over a wide range of pressures and flow rates," *IEEE Trans. Plasma Sci.*, vol. PS-6, pp. 341–354, Dec. 1978.

[2] S. Li, C. Akyel, and R. G. Bosisio, "Precise calculations and measurements on the complex dielectric constant of lossy materials using $TM_{010}$ cavity perturbation techniques," *IEEE Trans. Microwave Theory Tech.*, vol. MTT-29, pp. 1041–1047, Oct. 1981.

[3] Shuh-han Chao, "Measurements of microwave conductivity and dielectric constants by the cavity perturbation method and their errors," *IEEE Trans. Microwave Theory Tech.*, vol. MTT-33, pp. 519–526, June 1985.

[4] R. R. Bonetti and A. E. Atia, "Design of cylindrical dielectric resonators in inhomogeneous media," *IEEE Trans. Microwave Theory Tech.*, vol. MTT-29, pp. 323–326, Apr. 1981.

[5] K. A. Zaki and A. E. Atia, "Modes in dielectric-loaded waveguides and resonators," *IEEE Trans. Microwave Theory Tech.*, vol. MTT-31, pp. 1039–1045, Dec. 1983.

[6] K. Solbach and I. Wolff, "The electromagnetic fields and phase constants of dielectric image lines," *IEEE Trans. Microwave Theory Tech.*, vol. MTT-26, pp. 266–274, Apr. 1978.

[7] A. K. Tiwari, B. Bhat, and R. P. Singh, "Generalized coupled dielectric waveguide and its variants for millimeter-wave applications," *IEEE Trans. Microwave Theory Tech.*, vol. MTT-34, pp. 869–875, Aug. 1986.

[8] El-Deek M. El-Sayed and M. N Morsy, "Use of transmission-line matrix method in determining the resonant frequencies of loaded microwave ovens," *J. Microwave Power*, vol. 19, no. 1, pp. 65–71, 1984.

[9] H. Y. Yee and N. F. Audeh, "Uniform waveguides with arbitrary cross-section considered by the point-matching method," *IEEE Trans. Microwave Theory Tech.*, vol. MTT-13, pp. 847–851, Nov. 1965.

[10] J. E. Goell, "A circular-harmonic computer analysis of rectangular dielectric waveguides," *Bell Syst. Tech. J.*, vol. 48, pp. 2133–2161, Sept. 1969.

[11] E. Yamashita, K. Atsuki, O. Hashimoto, and K. Kamijo, "Modal analysis of homogeneous optical fibers with deformed boundaries," *IEEE Trans. Microwave Theory Tech.*, vol. MTT-27, pp. 352–356, Apr. 1979.

[12] S. Ramo, J. R. Whinnery, and T. Van Duzer, *Fields and Waves in Communication Electronics*. New York: Wiley, 1984.

[13] R. F. Harrington, *Time-Harmonic Electromagnetic Fields*. New York: McGraw-Hill, 1961.

[14] P. J. B. Clarricoats, "Backward-waves in waveguides containing dielectric," *Proc. Inst. Elec. Eng.*, vol. C108, pp. 496–501, June 1961.

[15] W. O. Schlosser and H. G. Unger, "Partially filled waveguides and surface waveguides of rectangular cross section," in *Advances in Microwaves*, vol. 1. New York: Academic Press, 1966, pp. 319–387.
[16] A. S. Omar and K. Schunemann, "Complex and backward-wave modes in inhomogeneously and anisotropically filled waveguides," *IEEE Trans. Microwave Theory Tech.*, vol. MTT-35, pp. 268–275, Mar. 1987.
[17] M. A. Rzepecka and A. K. Hamid, "Modified perturbation method for permittivity measurements at microwave frequencies," *J. Microwave Power*, vol. 9, no. 4, pp. 317–328, 1974.

✠

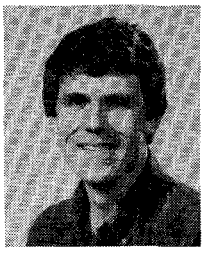

**Edward J. Rothwell** (S'84–M'85) was born in Grand Rapids, MI, on September 8, 1957. He received the B.S. degree in electrical engineering from Michigan Technological University Houghton, in 1979 and the M.S. in electrical engineering and the degree of electrical engineer from Stanford University, Stanford, CA, in 1980 and 1982. In 1985 he received the Ph.D. degree in electrical engineering from Michigan State University, East Lansing, where he held the Dean's Distinguished Fellowship.

He worked for Raytheon Company, Microwave and Power Tube Division, Waltham, MA, from 1979 to 1982 on low-power traveling wave tubes. Since 1985 he has been at Michigan State University, East Lansing, as an Assistant Professor of Electrical Engineering.

Dr. Rothwell is a member of Phi Kappa Phi.

✠

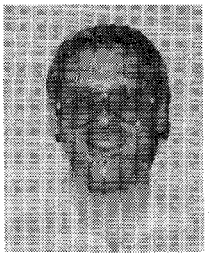

**Lydell L. Frasch** (S'87) received the B.S. degree in physics in 1979 and the B.S. degree in electrical engineering in 1980, both from the South Dakota School of Mines and Technology, Rapid City. He joined the Dow Chemical Company in 1980, where he was involved in the design and specification of analytical instrument systems. In 1984 he received the M.S. degree in electrical engineering from Michigan State University, where he is currently pursuing a doctorate in electrical engineering.